

Standard siren cosmology in the era of the 2.5-generation ground-based gravitational wave detectors: bright and dark sirens of LIGO Voyager and NEMO

Shang-Jie Jin,^a Rui-Qi Zhu,^a Ji-Yu Song,^a Tao Han,^a Jing-Fei Zhang^a and Xin Zhang^{a,b,c,1}

^aKey Laboratory of Cosmology and Astrophysics (Liaoning Province) and College of Sciences, Northeastern University, Shenyang 110819, China

^bKey Laboratory of Data Analytics and Optimization for Smart Industry (Ministry of Education), Northeastern University, Shenyang 110819, China

^cNational Frontiers Science Center for Industrial Intelligence and Systems Optimization, Northeastern University, Shenyang 110819, China

E-mail: jinshangjie@stumail.neu.edu.cn, zhuruiqi@stumail.neu.edu.cn,
songjiyu@stumail.neu.edu.cn, hantao@stumail.neu.edu.cn,
jfzhang@mail.neu.edu.cn, zhangxin@mail.neu.edu.cn

Abstract. The 2.5-generation (2.5G) ground-based gravitational wave (GW) detectors LIGO Voyager and NEMO are expected to be operational in the late 2020s and early 2030s. In this work, we explore the potential of GW standard sirens observed by the 2.5G GW detectors in measuring cosmological parameters, especially for the Hubble constant. Using GWs to measure cosmological parameters is inherently challenging, especially for 2.5G detectors, given their limited capability, which results in weaker constraints on cosmological parameters from the detected standard sirens. However, the measurement of the Hubble constant using standard siren observations from Voyager and NEMO is still promising. For example, using bright sirens from Voyager and NEMO can measure the Hubble constant with an accuracy of about 2% and 6% respectively, and using the Voyager-NEMO network can improve the accuracy to about 1.6%. Moreover, bright sirens can be used to break the degeneracy of cosmological parameters generated by CMB data, and to a certain extent, 2.5G detectors can also play a role in this aspect. Observations of dark sirens by 2.5G detectors can achieve relatively good results in measuring the Hubble constant, with an accuracy of within 2%, and if combining observations of bright and dark sirens, the accuracy of the Hubble constant measurement can reach about 1.3%. Finally, we also discussed the impact of the uncertainty in the binary neutron star merger rate on the estimation of cosmological parameters. We conclude that the magnificent prospect for solving the Hubble tension is worth expecting in the era of the 2.5G ground-based GW detectors.

¹Corresponding author.

Contents

1	Introduction	1
2	Methodology	2
2.1	Simulations of GW events	2
2.2	Detections of GW events	3
2.3	Estimations of GW parameters	6
2.4	Bright sirens: detections of SGRBs and inferences of cosmological parameters	7
2.5	Galaxy localization	9
2.6	Dark sirens: Bayesian inferences of cosmological parameters	9
3	Results and discussions	11
3.1	Bright sirens	12
3.2	Dark sirens	15
3.3	Impact of uncertainty in the BNS merger rate on estimating cosmological parameters	16
3.4	Impact of the detector coordinates in the antenna response functions on estimating the Hubble constant in the dark siren scenario	18
4	Conclusion	19

1 Introduction

In recent decades, the study of cosmology has achieved great success. The Λ cold dark matter (Λ CDM) model, which is now viewed as the standard model of cosmology, has been established and strongly favors the current observations. In particular, based on the standard Λ CDM model, the precise measurements of cosmic microwave background (CMB) anisotropies have ushered in the era of precision cosmology [1, 2]. However, in recent years, with the improvements of the measurement precisions of cosmological parameters, some puzzling tensions appear. Notably, the tension between the values of the Hubble constant inferred from the Planck CMB observations (0.8% precision, assuming the Λ CDM model) [3] and obtained through distance ladder measurements (1.4% measurement, model-independent) [4] has now reached more than 5σ [4]. Recently, the Hubble tension has been widely discussed in the literature [5–25]. The Hubble tension may imply the possibility of new physics beyond the standard model of cosmology. However, there is currently no consensus on a definitive extended cosmological model that can effectively resolve the Hubble tension. On the other hand, it is also important to develop late-universe cosmological probes that can independently measure the Hubble constant to make an arbitration for the Hubble tension. The gravitational wave (GW) standard siren method is one of the most promising methods.

The absolute luminosity distance can be directly obtained through the analysis of the GW waveform, which is called a standard siren [26, 27]. If the redshift information could also be obtained by identifying electromagnetic (EM) counterparts (this type of standard sirens are typically referred to as “bright sirens”) or statistically from cross-correlation of GW and galaxy catalogs (this type of standard sirens are typically referred to as “dark sirens”), the distance-redshift relation could be used to explore the expansion history of the universe, which

is widely discussed in the literature [28–70]. The landmark event of the first detected binary neutron star (BNS) merger event, GW170817, together with its EM counterparts, initiated the era of multi-messenger astronomy [71, 72]. The only bright siren event has given the first measurement of the Hubble constant with a precision of 14% [73]. For the dark sirens, the latest constraint precision of the Hubble constant given by LIGO-Virgo-KAGRA is 19% [74]. Neither method is sufficient to resolve the Hubble tension conclusively. Consequently, future observations and next-generation observatories will be crucial in shedding light on solving the Hubble tension.

The 2.5-generation (2.5G) GW observatories, LIGO Voyager [75] (abbreviated as Voyager hereafter) and Neutron Star Extreme Matter Observatory (NEMO) [76], will begin observing in the late 2020s and early 2030s. Voyager and NEMO would improve the detection sensitivity by a factor of about 5 over the current aLIGO, which can greatly improve the detection rates of compact binary coalescences [77]. Furthermore, Voyager and NEMO are expected to form a detector network, which can improve the ability to localize GW sources. Therefore, the standard siren observations in the era of the 2.5G GW detectors may play an important role in cosmological parameter estimations, especially for measuring the Hubble constant.

Recently, GW astronomy in the 2.5G GW detector era was discussed in, e.g., refs. [77–81]. However, a detailed analysis of the GW standard siren observations from the 2.5G GW detectors in the cosmological parameter estimations is still absent and needs to be further discussed. Therefore, in this work, we wish to investigate the potential of the 2.5G GW detectors by considering three detection strategies: Voyager, NEMO, and the Voyager-NEMO network, to address three key questions: (i) what precisions the cosmological parameters could be measured using the bright sirens of 2.5G GW detectors, (ii) what role the bright sirens of 2.5G GW detectors could play in helping break the cosmological parameter degeneracies generated by the EM observations, and (iii) what precision the Hubble constant could be measured using the dark sirens of 2.5G GW detectors. Through our analysis, we aim to shed light on these aspects and explore the potential role of 2.5G GW detectors in helping solve the Hubble tension and advancing our understanding of cosmology.

This work is organized as follows. In section 2, we introduce the methodology of simulating bright and dark siren data. In section 3, we give the constraint results and make some relevant discussions. The conclusion is given in section 4. Throughout this work, we adopt the flat Λ CDM model as the fiducial model to generate the mock standard siren data with $\Omega_m = 0.3166$ and $H_0 = 67.27 \text{ km s}^{-1} \text{ Mpc}^{-1}$ from the constraint results of Planck 2018 TT,TE,EE+lowE [3].

2 Methodology

2.1 Simulations of GW events

In the observation frame, the merger rate as a function of the redshift is given by

$$R_{\text{obs}}(z) = \frac{R_{\text{m}}(z) dV(z)}{1+z dz}, \quad (2.1)$$

where the $(1+z)$ term arises from converting the source-frame time to the observation-frame time and dV/dz is the comoving volume element. R_{m} is the source-frame merger rate, which

is related to the cosmic star formation rate,

$$R_m(z_m) = \int_{z_m}^{\infty} dz_f \frac{dt_f}{dz_f} R_{\text{sf}}(z_f) P(t_d), \quad (2.2)$$

where t_m (or redshift z_m) is the lookback time corresponding to the merger of binary systems, t_f (or redshift z_f) represents the time when binary systems form, and the time-delay distribution $P(t_d)$ represents the probability density of the binary system formed at time t_f and merged at time t_m , with $t_d = t_m - t_f$. The cosmic star formation rate (SFR) R_{sf} is assumed the Madau-Dickinson SFR [82], with an exponential time delay [83].

In the present work, we simulate the BNS and binary black hole (BBH) mergers for the following discussions. For BNS mergers, we consider the local comoving merger rate $R_m(0)$ to be $R_m(0) = 320 \text{ Gpc}^{-3} \text{ yr}^{-1}$, which is the estimated median rate based on the O3a observation [84]. While for BBH mergers, we consider $R_m(0) = 23.9 \text{ Gpc}^{-3} \text{ yr}^{-1}$, which is the estimated median rate of O2 observation [85] and is also consistent with the O3 observation [86].

The sky location (θ, ϕ) , the binary inclination angle ι , the polarization angle ψ , and the coalescence phase ψ_c are randomly sampled in the ranges of $\cos\theta \in [-1, 1]$, $\phi \in [0, 2\pi]$, $\cos\iota \in [-1, 1]$, $\psi \in [0, 2\pi]$, and $\psi_c \in [0, 2\pi]$, respectively. The coalescence time t_c is chosen as $t_c \in [0, 10]$ years for both bright and dark sirens. For the mass distribution, we employ the numerical fitting formulas to fit the curves shown in figure 7 of the POWER PEAK population model (mass of NS in the range of $[1.2, 2] M_{\odot}$) in ref. [86] for NS and the POWER LAW + PEAK model (mass of BH in the range of $[5, 44] M_{\odot}$) in refs. [85, 86] for BH. Note that in the present work, all the simulated BNS mergers will be used for the bright siren analysis, while all the BBH mergers will be used for the dark siren analysis.

2.2 Detections of GW events

In this work, we consider the phenomenological non-spinning inspiral-merger-ringdown PhenmonA model [87, 88]. The frequency-domain GW waveform is given by

$$\tilde{h}(f) = \mathcal{A} \exp[i(2\pi f t_c - \pi/4 - 2\psi_c + 2\Psi(f/2) - \varphi_{(2,0)})], \quad (2.3)$$

where the amplitude \mathcal{A} is given by

$$\mathcal{A} = \mathcal{A}_{\text{eff}} \begin{cases} \left(\frac{f}{f_0}\right)^{-7/6}, & f < f_0, \\ \left(\frac{f}{f_0}\right)^{-2/3}, & f_0 \leq f < f_1, \\ \omega \mathcal{L}(f, f_1, f_2), & f_1 \leq f < f_3, \end{cases} \quad (2.4)$$

and the form of \mathcal{A}_{eff} is written as

$$\mathcal{A}_{\text{eff}} = \frac{1}{d_L} \sqrt{F_+^2 (1 + \cos^2(\iota))^2 + 4F_{\times}^2 \cos^2(\iota)} \times \sqrt{5\pi/96} \mathcal{M}_{\text{chirp}}^{5/6} (\pi f_0)^{-7/6}, \quad (2.5)$$

$\Psi(f)$ and $\varphi_{(2,0)}$ are given by [89, 90]

$$\Psi(f) = \frac{3}{256\eta} \sum_{i=0}^7 \alpha_i (2\pi M f)^{(i-5)/3}, \quad (2.6)$$

$$\varphi_{(2,0)} = \tan^{-1} \left(-\frac{2 \cos(\iota) F_{\times}}{(1 + \cos^2(\iota)) F_+} \right), \quad (2.7)$$

where d_L is the luminosity distance to the GW source, ι is the inclination angle between the orbital angular momentum axis of the binary and the line of sight, $\mathcal{M}_{\text{chirp}}$ is the observed chirp mass which is defined as $\mathcal{M}_{\text{chirp}} = (1+z)M\eta^{3/5}$, $M = m_1 + m_2$ is the total mass of the binary system, $\eta = m_1 m_2 / (m_1 + m_2)^2$ is the symmetric mass ratio, t_c is the coalescence time, ψ_c is the coalescence phase, and the coefficients α_i (we calculate the GW waveform to the 3.5 PN order) are detailedly given in e.g., refs. [89, 91]. Note that f_0 is the merger frequency, f_1 is the ringdown frequency, f_2 is the decay-width of the ringdown, f_3 is the cut-off frequency, and the forms of ω and \mathcal{L} are related to f_0 , f_1 , and f_2 . The forms of f_0 , f_1 , f_2 , f_3 , ω , and \mathcal{L} are detailedly introduced in e.g., table 2 and eqs. (21)–(23) of ref. [92].

Here F_+ and F_\times are the antenna response functions of the detector, which are related to the location of the GW source (θ , ϕ) and the polarization angle ψ . For Voyager and NEMO, the antenna response functions are

$$\begin{aligned} F_+(\theta, \phi, \psi) &= \frac{1}{2}(1 + \cos^2(\theta)) \cos(2\phi) \cos(2\psi) - \cos(\theta) \sin(2\phi) \sin(2\psi), \\ F_\times(\theta, \phi, \psi) &= \frac{1}{2}(1 + \cos^2(\theta)) \cos(2\phi) \sin(2\psi) + \cos(\theta) \sin(2\phi) \cos(2\psi). \end{aligned} \quad (2.8)$$

Note that when considering the detector network in the GW localization, it is optimal to consider the detailed detector coordinates in the antenna response functions. However, the coordinates of the 2.5G GW detectors are currently uncertain. Therefore, the above forms of $F_{+,\times}$ are adopted without considering the detector locations. In section 3.4, we discuss the impact of the detector coordinates in the antenna response functions on the cosmological analysis.

The signal-to-noise ratio (SNR) of the detector is given by

$$\rho = (\tilde{h}|\tilde{h})^{1/2}, \quad (2.9)$$

with the inner product being defined as

$$(a|b) = 2 \int_{f_{\text{lower}}}^{f_{\text{upper}}} \frac{a(f)b^*(f) + a^*(f)b(f)}{S_n(f)} df, \quad (2.10)$$

where f_{lower} is the lower-frequency cutoff, f_{lower} is chosen as $f_{\text{lower}} = \max(f_{\text{obs}}, 5)$ Hz for NEMO and $f_{\text{lower}} = \max(f_{\text{obs}}, 10)$ Hz for Voyager, $f_{\text{obs}} = (t_c/5)^{-3/8} \mathcal{M}_{\text{chirp}}^{-5/8} / 8\pi$ is the observation frequency at the coalescence time t_c , $f_{\text{upper}} = f_3$ is the upper-frequency cutoff, $*$ denotes the complex conjugate, and $S_n(f)$ is the one-side noise power spectral density (PSD). We adopt the forms of PSDs for NEMO from ref. [76] and Voyager from ref. [93], as shown in figure 1. The SNR threshold is set to 8 for bright sirens and 100 for dark sirens.

In figure 2, we show the corresponding detection horizons ($\text{SNR} \geq 8$) for equal-mass non-spinning binaries as a function of the source frame total mass for Voyager and NEMO. We can see that the detection capability of Voyager for compact binary coalescences is better than that of NEMO.

In figure 3, we show the redshift distributions of the GW events detected by the Voyager-NEMO network, assuming the 10-year observation. We can see that the Voyager-NEMO network can detect BNS mergers at $z < 0.5$. The detailed detection numbers are shown in table 1.

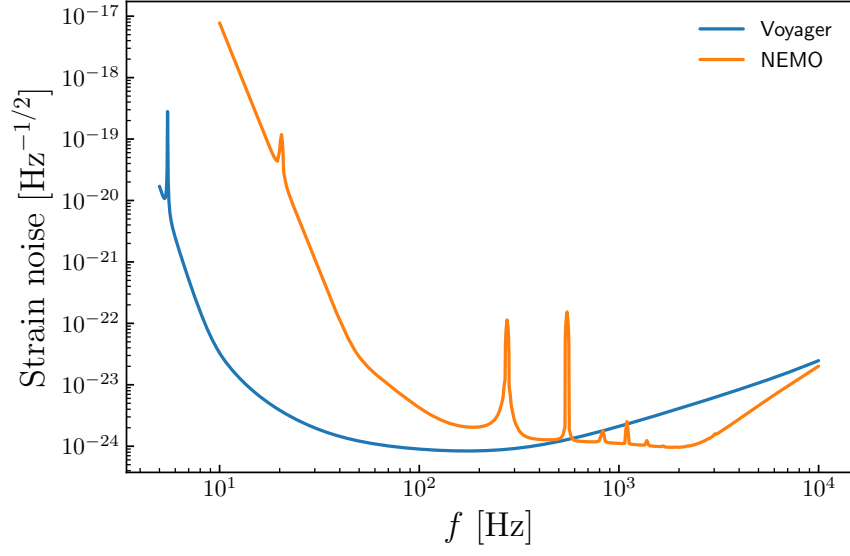


Figure 1. Sensitivity curves of Voyager and NEMO adopted in this work.

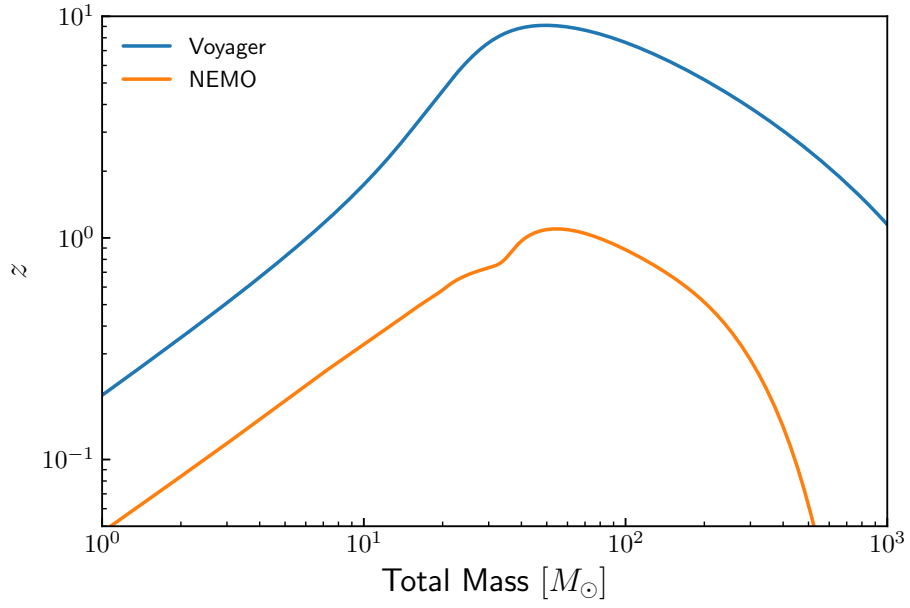


Figure 2. Detection horizons for the equal-mass non-spinning binaries as a function of the source frame total mass for Voyager and NEMO.

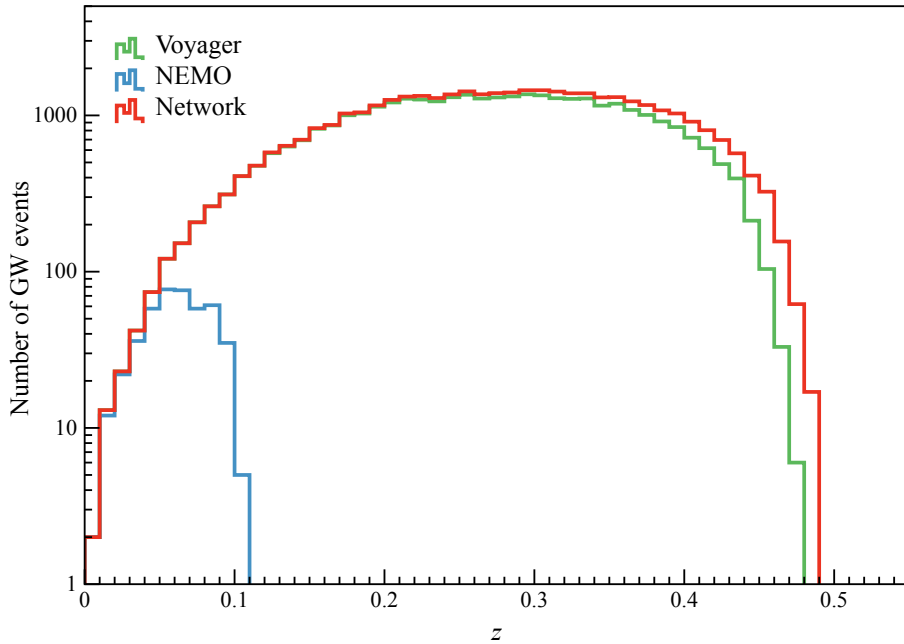


Figure 3. Redshift distributions of the BNS merger events detected by Voyager, NEMO, and the Voyager-NEMO network based on the 10-year observation.

2.3 Estimations of GW parameters

We use the Fisher information matrix to estimate the measurement errors of the GW parameters. For a set of parameters $\boldsymbol{\theta}$, the Fisher information matrix is given by

$$F_{ij} = \left(\frac{\partial \tilde{h}}{\partial \theta_i} \middle| \frac{\partial \tilde{h}}{\partial \theta_j} \right), \quad (2.11)$$

where $\boldsymbol{\theta}$ denotes nine GW parameters (d_L , $\mathcal{M}_{\text{chirp}}$, η , t_c , ψ_c , ι , θ , ϕ , ψ) for a binary system. The covariance matrix is equal to the inverse of the Fisher information matrix, i.e., $\text{Cov}_{ij} = \sqrt{(F^{-1})_{ij}}$. Then the measurement errors of the GW parameters is $\Delta\theta_i = \sqrt{(F^{-1})_{ii}}$.

The sky localization error is given by

$$\Delta\Omega = 2\pi |\sin\theta| \sqrt{(\Delta\theta)^2 (\Delta\phi)^2 - (\Delta\theta\Delta\phi)^2}, \quad (2.12)$$

where $\Delta\theta$, $\Delta\phi$, and $\Delta\theta\Delta\phi$ can be calculated by the covariance matrix.

In addition to the measurement error caused by the GW observation, the errors from weak lensing and peculiar velocity are also considered. For the error caused by weak lensing, we adopt the form [94–96]

$$\sigma_{d_L}^{\text{lens}}(z) = \left[1 - \frac{0.3}{\pi/2} \arctan(z/0.073) \right] \times d_L(z) \times 0.066 \left[\frac{1 - (1+z)^{-0.25}}{0.25} \right]^{1.8}. \quad (2.13)$$

The error caused by peculiar velocity is given by [97]

$$\sigma_{d_L}^{\text{pv}}(z) = d_L(z) \times \left[1 + \frac{c(1+z)^2}{H(z)d_L} \right] \frac{\sqrt{\langle v^2 \rangle}}{c}, \quad (2.14)$$

where $H(z)$ is the Hubble parameter, $\sqrt{\langle v^2 \rangle}$ is the peculiar velocity of the GW source, and c is the speed of light in vacuum. Here we set $\sqrt{\langle v^2 \rangle} = 500 \text{ km s}^{-1}$, in agreement with the average value observed in galaxy catalogs [98]. Hence, the total error of d_L can be written as

$$(\sigma_{d_L})^2 = (\sigma_{d_L}^{\text{inst}})^2 + (\sigma_{d_L}^{\text{lens}})^2 + (\sigma_{d_L}^{\text{pv}})^2. \quad (2.15)$$

2.4 Bright sirens: detections of SGRBs and inferences of cosmological parameters

In this subsection, we introduce the method of simulating the joint GW and short γ -ray burst (SGRB) events and performing cosmological analysis. We consider the THESEUS-like GRB detector in synergy with the 2.5G GW observation.

For the SGRB model, we consider the model of Gaussian-structure jet profile based on the GW170817/GRB170817A observation,

$$L_{\text{iso}}(\theta_V) = L_{\text{on}} \exp\left(-\frac{\theta_V^2}{2\theta_c^2}\right), \quad (2.16)$$

where $L_{\text{iso}}(\theta)$ is the isotropic equivalent luminosity of SGRB at the viewing angle θ_V , L_{on} is the on-axis isotropic luminosity defined by $L_{\text{on}} = L_{\text{iso}}(0)$, and $\theta_c = 4.7^\circ$ is the characteristic angle of the core. The direction of the jet is assumed to coincide with the direction of the angular momentum of the binary's orbital motion, i.e., $\iota = \theta_V$.

The SGRB detectors are limited by the flux sensitivity for the distant GRB emissions at wider viewing angles. For the THESEUS-like detector, the sensitivity flux limit is $P_T = 0.2 \text{ ph s}^{-1} \text{ cm}^{-2}$, in the 50-300 keV band. According to the relation between flux and luminosity for GRB [99, 100], we can convert the flux limit P_T to the luminosity by

$$L_{\text{iso}} = 4\pi d_L^2(z) k(z) b / (1+z) P_T, \quad (2.17)$$

where $k(z)$ is the k -correction form and is given by

$$k(z) = \int_{E_1}^{E_2} N(E) dE / \int_{E_1(1+z)}^{E_2(1+z)} N(E) dE, \quad (2.18)$$

b is an energy normalization and is given by

$$b = \int_{1 \text{ keV}}^{10000 \text{ keV}} EN(E) dE / \int_{E_1}^{E_2} N(E) dE, \quad (2.19)$$

where $[E_1, E_2]$ is the detector's energy window, i.e., $E_1 = 50 \text{ keV}$ and $E_2 = 300 \text{ keV}$. The observed photon flux is scaled by b to account for the missing fraction of the γ -ray energy seen in the detector band. The cosmological k -correction is due to the redshifted photon energy when traveling from source to detector. $N(E)$ is the observed GRB photon spectrum in units of $\text{ph s}^{-1} \text{ keV}^{-1} \text{ cm}^{-2}$. For SGRBs, the function $N(E)$ is simulated by the Band function [101] which is a function of spectral indices (α_B, β_B) and break energy E_b ,

$$N(E) = \begin{cases} N_0 \left(\frac{E}{100 \text{ keV}}\right)^{\alpha_B} \exp\left(-\frac{E}{E_0}\right), & E \leq E_b, \\ N_0 \left(\frac{E_b}{100 \text{ keV}}\right)^{\alpha_B - \beta_B} \exp(\beta_B - \alpha_B) \left(\frac{E}{100 \text{ keV}}\right)^{\beta_B}, & E > E_b, \end{cases} \quad (2.20)$$

Table 1. Estimated numbers of the GW events detected by Voyager, NEMO, and the Voyager-NEMO network, and the joint GW-GRB events detected by THESEUS-like GRB detector, assuming the 10-year observation.

Detection strategy	GW events	GW-GRB events
Voyager	35715	42
NEMO	442	5
Network	39249	50

where $E_b = (\alpha_B - \beta_B)E_0$ and $E_p = (\alpha_B + 2)E_0$. Here we adopt $\alpha_B = -0.5$, $\beta_B = -2.25$, and a peak energy $E_p = 800$ keV in the source frame from ref. [102]. This is a phenomenological fit to the observed spectra of GRB prompt emissions.

Finally, we could calculate the detection probability of SGRBs. The detection probability of an SGRB is determined by $\Phi(L)dL$, where $\Phi(L)$ is the intrinsic luminosity function and L is the peak luminosity of each burst, which is assumed to be isotropically emitted in the rest frame in the energy range of 1 – 10000 keV. For the luminosity function, we assume a standard broken power law of the form when considering the SGRB

$$\Phi(L) = \begin{cases} \left(\frac{L}{L^*}\right)^{\alpha_L}, & L < L^*, \\ \left(\frac{L}{L^*}\right)^{\beta_L}, & L > L^*, \end{cases} \quad (2.21)$$

where L^* is the characteristic luminosity that separates the low and high ends of the luminosity function. Following ref. [102], we adopt the characteristic slopes $\alpha_L = -1.95$, $\beta_L = -3$ and $L^* = 2 \times 10^{52}$ erg s⁻¹ to describe the characteristic luminosity for different regimes. Finally, for each BNS sample, we could select the SGRB detections from the BNS samples by calculating the probability of the detection P

$$P = \int_{L_c}^{\infty} \Phi(L)dL. \quad (2.22)$$

We emphasize that we make an optimistic assumption that all the detectable GW-GRB events can provide redshift measurements. According to the calculations, the numbers of the simulated bright sirens from Voyager, NEMO, and the Voyager-NEMO network is 42, 5, and 50, respectively, based on the 10-year observation, as shown in table 1. The numbers of GW-GRB events from Voyager and NEMO are also consistent with those given in refs. [78, 103]. Similar discussions but for the third-generation (3G) GW detectors are also discussed in e.g., refs. [67, 104]. For example, compared to the results reported in ref. [67], we see that the numbers of detected GW events from the 3G GW detectors are two orders of magnitudes greater than the 2.5G result, and the number of the 3G GW-GRB events exceeds the 2.5G results by one order of magnitude.

For the cosmological parameter estimations using the mock bright siren data, we adopt the Markov-chain Monte Carlo analysis to maximize the likelihood $\mathcal{L} \propto (-\chi^2/2)$ and infer the posterior probability distributions of cosmological parameters $\vec{\Omega}$. The χ^2 function is defined as

$$\chi^2 = \sum_{i=1}^N \left(\frac{\hat{d}_{L,i} - d_L(z_i, \vec{\Omega})}{\sigma_{d_{L,i}}} \right)^2, \quad (2.23)$$

where N is the number of the bright siren data. We use the `emcee` Python module [105] to constrain the cosmological parameters.

2.5 Galaxy localization

We first obtain the sky localization errors and luminosity distance errors of BBHs. For the simulation of galaxy catalogs, we uniformly simulate in a co-moving volume with a number density of 0.02 Mpc^{-3} in the range of $z \in [0, 0.2]$ (note that the adopted galaxy number is in the middle of the observational error bars, see figure 1 of ref. [106] for more details). By combining the flat priors for $\Omega_m \in [0.1, 0.5]$ and $H_0 \in [60, 80]$, and the luminosity distance errors, we obtain the lower and upper limits of redshift (z_{\min}, z_{\max}), assuming the Λ CDM model. We then derive the 2×2 covariance matrix Cov including θ and ϕ from the whole covariance matrix and use the new covariance matrix to calculate χ^2 , which describes the angular deviation from an arbitrary galaxy to the GW source and is given by

$$\chi^2 = \boldsymbol{\xi} (\text{Cov}^{-1}) \boldsymbol{\xi}^\top = \sum_{i,j} \xi_i (\text{Cov}^{-1})_{ij} \xi_j, \quad (2.24)$$

with $\boldsymbol{\xi} = (\theta - \bar{\theta}, \phi - \bar{\phi})$. Here $(\bar{\theta}, \bar{\phi})$ represent the angular location of the GW source, and (θ, ϕ) represent the angular location of an arbitrary galaxy. We adopt the boundary of the GW source's angular localization with $\chi^2 = 9.21$, corresponding to the 99% confidence level. Therefore, if the galaxies satisfy $\chi^2 \leq 9.21$ and $z \in [z_{\min}, z_{\max}]$, they can be considered as the potential host galaxies of the GW source.

2.6 Dark sirens: Bayesian inferences of cosmological parameters

For the GW events that cannot identify EM counterparts to determine the redshift information, we need to use the cross-correlation of GW localization and galaxy catalogs to obtain redshift information. In this subsection, we briefly introduce the method of using the dark siren method to infer the cosmological parameters. Using the method introduced in section 2.5, we calculate the number of the potential host galaxies N_{in} and show the SNR– N_{in} plot in figure 4. We can see that the higher the SNR of the GW event, the smaller the number of host galaxies N_{in} . Meanwhile, the GW events with lower SNRs mainly have higher redshifts.

We use the following Bayesian method and the `emcee` Python module [105] to constrain the cosmological parameters. Here we consider the future galaxy survey projects, e.g., the China Space Station Telescope, which are anticipated to yield a galaxy catalog with a completeness level of 100% at redshifts $z \leq 0.3$ [60]. Hence, we do not consider the galaxy catalog's incompleteness in the following methods, as we only use GW events with $z < 0.15$. The posterior probability distribution of the cosmological parameters $\vec{\Omega}$ is

$$p(\vec{\Omega} | \vec{X}_{\text{GW}}) \propto p(\vec{\Omega}) \mathcal{L}(\vec{X}_{\text{GW}} | \vec{\Omega}), \quad (2.25)$$

where $p(\vec{\Omega})$ are the prior distributions of the cosmological parameters and \vec{X}_{GW} represent the GW data. Assuming that the GW events are independent of each other, the likelihood of the GW data can be expressed as

$$\mathcal{L}(\vec{X}_{\text{GW}} | \vec{\Omega}) = \prod_{i=1}^{N_{\text{GW}}} \mathcal{L}(X_{\text{GW},i} | \vec{\Omega}), \quad (2.26)$$

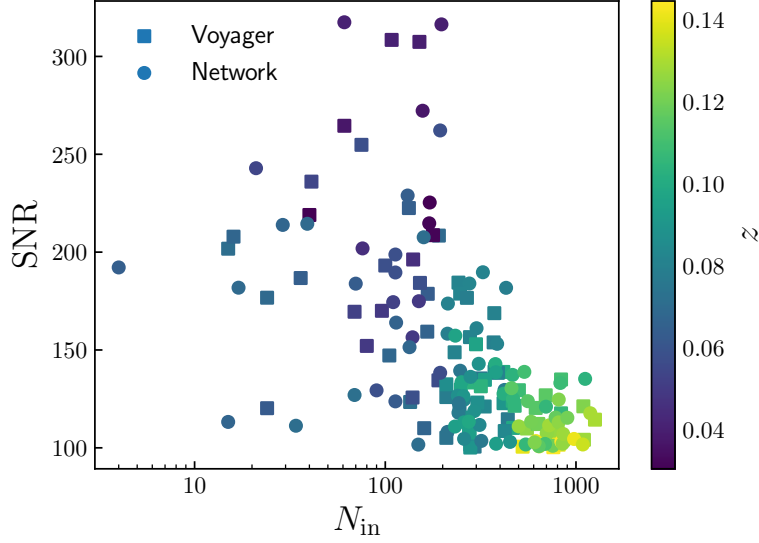


Figure 4. Correlation between SNRs of dark sirens from Voyager and the Voyager-NEMO network, the number of the potential host galaxies N_{in} , and redshifts of dark sirens based on the 10-year observation.

where N_{GW} is the number of GW events. The likelihood function $\mathcal{L}(X_{\text{GW}}|\vec{\Omega})$ is obtained by marginalizing the redshifts of the GW events,

$$\mathcal{L}(X_{\text{GW}}|\vec{\Omega}) = \int p(X_{\text{GW}}|d_{\text{L}}(z, \vec{\Omega}))p_z(z)dz, \quad (2.27)$$

where $p(X_{\text{GW}}|d_{\text{L}}(z, \vec{\Omega}))$ is the posterior distribution of GW event's d_{L} obtained from the GW observation and is given by

$$p(X_{\text{GW}}|d_{\text{L}}(z, \vec{\Omega})) = \frac{1}{\sqrt{2\pi}\sigma_{d_{\text{L}}}} \exp\left[-\frac{(\hat{d}_{\text{L}} - d_{\text{L}}(z, \vec{\Omega}))^2}{2\sigma_{d_{\text{L}}}^2}\right], \quad (2.28)$$

where \hat{d}_{L} is the observed luminosity distance of the GW source and the luminosity distance error $\sigma_{d_{\text{L}}}$ can be obtained from eq. (2.15). $p_z(z)$ are the prior distributions of the redshifts of GW sources and can be expressed as,

$$p_z(z) \propto \frac{1}{N_{\text{in}}} \sum_{n=1}^{N_{\text{in}}} W_n \delta(\hat{z}_n - z), \quad (2.29)$$

where $\delta(\hat{z}_n - z)$ is the delta function with \hat{z}_n being the redshift of the n -th potential host galaxy and W_n is the angular position weight of the n -th potential host galaxy

$$W_n \propto \exp\left(-\frac{1}{2}\chi_n^2\right). \quad (2.30)$$

Here χ_n^2 is obtained from eq. (2.24).

We emphasize that the application of dark siren in constraining cosmological parameters heavily relies on the localization ability, i.e., the number of potential host galaxies, as introduced in section 2.5. Therefore, we adopt the SNR threshold of dark sirens to be 100, which can ensure more precise localizations of dark sirens, thereby significantly reducing the number of potential host galaxies. According to the calculations of the 10-year observation, the detection numbers of BBH merger events are 83 and 93 for Voyager and the Voyager-NEMO network, respectively. Note that owing to the fact that NEMO is not sensitive to the GW signals from BBH mergers, we do not consider the single NEMO observatory in the dark siren analysis.

The GW selection effect is not considered in this work for simplicity. To account for the GW selection effect, it is necessary to normalize the likelihood of a single event using a selection function. This function is derived from the integrated likelihood of the single event across all datasets that are classified as detected according to the detection statistics [107]. Nevertheless, only dark sirens with $\text{SNR} \geq 100$ are considered, which can partially simplify the inference problem. Moreover, selection biases are subdominant compared to statistical uncertainties for the high-SNR events [69]. Although our approach might omit a number of GW events, we consider the analysis to be conservative due to the significant localization errors associated with low SNR events. These errors can lead to the identification of an excessive number of potential host galaxies. On one hand, such GW events with large localization errors could result in a weaker contribution to the estimations of cosmological parameters. On the other hand, it would increase computational time significantly (integration calculation with 10^5 or even more events). Therefore, we believe that our method, while potentially omitting some events, is a conservative approach.

3 Results and discussions

In this section, we shall report the constraint results of the cosmological parameters. To ensure a comprehensive and robust analysis of cosmological parameter estimations, we consider two scenarios, bright sirens (optimistic) and dark sirens (conservative). For the optimistic scenario, we use the simulated bright siren data to constrain the Λ CDM, w CDM, and w_0w_a CDM models. Furthermore, we consider three detection strategies, Voyager, NEMO, and the Voyager-NEMO network to make the following discussions. In order to show the ability of the bright sirens to break the cosmological parameter degeneracies generated by CMB, we also show the constraint results of CMB and the combination of GW and CMB. For the CMB data, we employ the ‘‘Planck distance priors’’ from the Planck 2018 observation [3, 108]. The constraint results for the cosmological parameters of interest are shown in figures 5–8 and summarized in table 2. We use $\sigma(\xi)$ and $\varepsilon(\xi)$ to represent the absolute and relative errors of parameter ξ , with $\varepsilon(\xi)$ defined as $\varepsilon(\xi) = \sigma(\xi)/\xi$. For the conservative scenario, we use the mock dark sirens from Voyager and the Voyager-NEMO network to constrain the Λ CDM model. The constraint results are shown in figure 9, and summarized in table 3. We discuss the impact of uncertainty in the BNS merger rate on estimating cosmological parameters. The related constraint results are shown in figures 10 and 11, and summarized in table 4. Furthermore, we also discuss the impact of the detector coordinates in the antenna response functions on estimating H_0 in the dark siren scenario, shown in figure 12 and summarized in table 5.

Table 2. The absolute errors (1σ) and the relative errors of the cosmological parameters in the Λ CDM, w CDM, and w_0w_a CDM models using the Voyager, NEMO, the Voyager-NEMO network, CMB, CMB+Voyager, CMB+NEMO, and CMB+Network data. Note that the mock GW data are based on the 10-year observation. Here H_0 is in units of $\text{km s}^{-1} \text{Mpc}^{-1}$.

Model	Error	Voyager	NEMO	Network	CMB	CMB+Voyager	CMB+NEMO	CMB+Network
Λ CDM	$\sigma(\Omega_m)$	–	–	–	0.0085	0.0079	0.0084	0.0073
	$\sigma(H_0)$	1.40	4.40	1.10	0.61	0.57	0.61	0.52
	$\varepsilon(\Omega_m)$	–	–	–	2.69%	2.49%	2.65%	2.30%
	$\varepsilon(H_0)$	2.08%	6.44%	1.63%	0.90%	0.85%	0.90%	0.77%
w CDM	$\sigma(\Omega_m)$	0.260	–	0.250	0.070	0.015	0.034	0.011
	$\sigma(H_0)$	2.25	4.15	1.75	7.75	1.50	3.50	1.10
	$\sigma(w)$	0.670	–	0.585	0.260	0.055	0.120	0.045
	$\varepsilon(\Omega_m)$	50.98%	–	54.35%	21.52%	4.72%	10.47%	3.47%
	$\varepsilon(H_0)$	3.40%	6.17%	2.63%	11.40%	2.23%	5.19%	1.63%
	$\varepsilon(w)$	72.83%	–	56.80%	25.74%	5.53%	12.05%	4.50%
w_0w_a CDM	$\sigma(\Omega_m)$	0.290	–	0.265	0.079	0.020	0.037	0.016
	$\sigma(H_0)$	2.60	4.40	1.95	9.00	2.00	4.05	1.60
	$\sigma(w_0)$	1.03	–	0.83	0.59	0.46	0.53	0.44
	$\sigma(w_a)$	–	–	–	–	1.70	–	1.60
	$\varepsilon(\Omega_m)$	55.77%	–	51.96%	24.84%	6.06%	11.56%	4.89%
	$\varepsilon(H_0)$	3.90%	6.48%	2.91%	13.04%	3.03%	6.01%	2.41%
	$\varepsilon(w_0)$	78.03%	–	60.14%	94.40%	88.46%	94.64%	67.69%

3.1 Bright sirens

In figure 5, we show the constraint results from Voyager, NEMO, and the Voyager-NEMO network. We can see that Network gives the best constraint results, followed by Voyager and NEMO. Since the GW-SGRB event number of Voyager is about 8 times more than that of NEMO, Voyager gives much better constraints than those of NEMO. Concretely, Voyager and NEMO give $\sigma(H_0) = 1.40 \text{ km s}^{-1} \text{Mpc}^{-1}$ and $\sigma(H_0) = 4.40 \text{ km s}^{-1} \text{Mpc}^{-1}$ with precisions of 2.08% and 6.44%, respectively. When considering the detector network, the constraint precision of H_0 is 21.4% and 75% better than those from the single Voyager and NEMO, respectively. Furthermore, when considering the Voyager-NEMO network, the constraint precision of H_0 is improved to 1.63%, which is close to the distance ladder measurement [4]. Therefore, in the 2.5G GW detector era, it is more meaningful to consider the detector network, i.e., the Voyager-NEMO network to perform cosmological analysis. In addition, the constraint precision of H_0 given by the 2.5G detector network is much better than the current constraint result given by the LIGO-Virgo-KAGRA observations [73, 74]. However, the constraint results are much worse than the forecast results by the 3G GW detectors (measurement precisions in the order of better than 1%) in e.g., refs. [42, 43, 45, 67]. Note that in the following we compare our bright siren results with those reported in ref. [67], which adopts the same bright siren analysis method as the present work. Since the Voyager-NEMO network gives the best constraints on cosmological parameters, we take the Voyager-NEMO network as the representative in the following discussions.

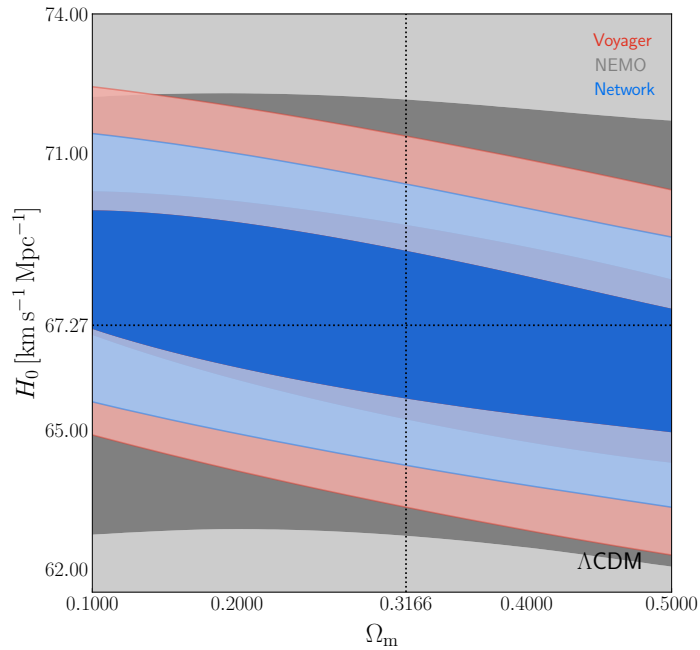


Figure 5. Two-dimensional marginalized contours (68.3% and 95.4% confidence level) in the Ω_m – H_0 plane using the 10-year mock bright siren data from Voyager, NEMO, and the Voyager-NEMO network in the Λ CDM model. Here, the dotted lines indicate the fiducial values of cosmological parameters preset in the simulation.

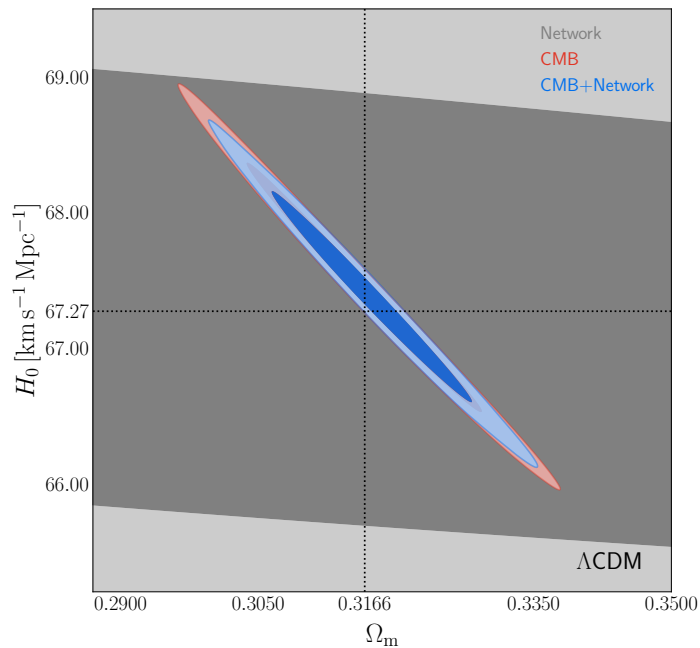


Figure 6. Same as figure 5, but using the Network, CMB, and CMB+Network data.

In figure 6, we show the constraint results in the Λ CDM model using the Network, CMB, and CMB+Network data. As clearly seen, bright sirens from the Voyager-NEMO

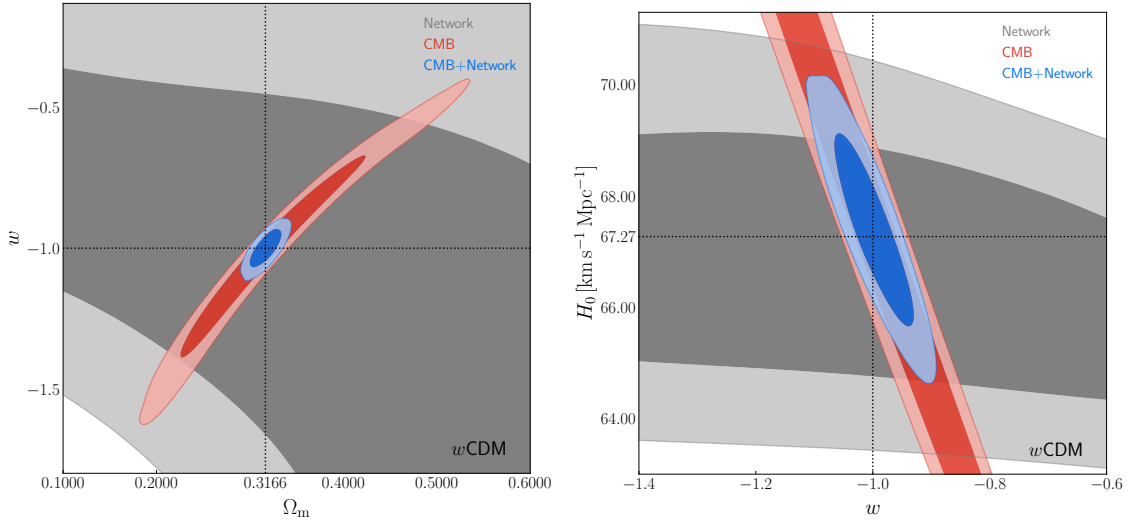


Figure 7. Same as figure 5, but for the w CDM model in the Ω_m - w and w - H_0 planes.

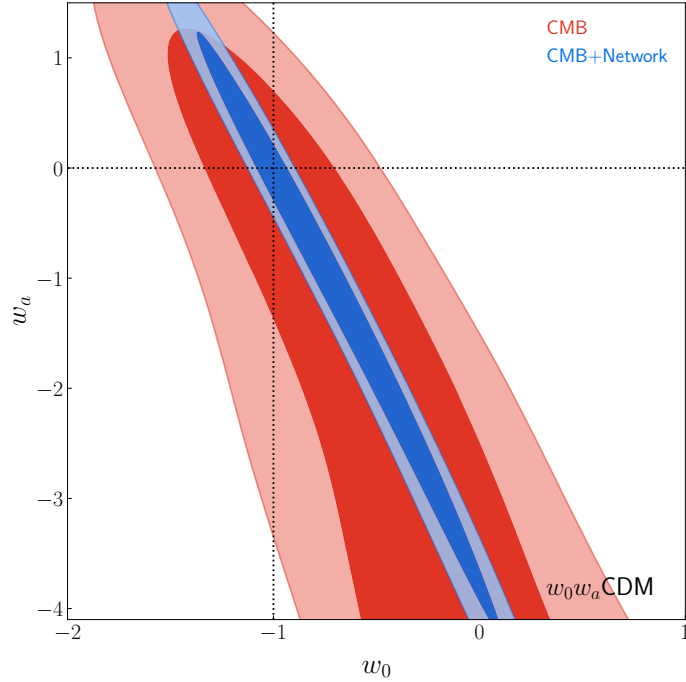


Figure 8. Same as figure 5, but using the CMB and CMB+Network data for the $w_0 w_a$ CDM model in the w_0 - w_a plane.

network can give tight constraint on H_0 , with a precision of 1.63%. Since GW could break the cosmological parameter degeneracies generated by CMB, the combination of them could improve the measurement precisions of cosmological parameters. The combination of CMB and Network gives $\sigma(\Omega_m) = 0.0073$ and $\sigma(H_0) = 0.52 \text{ km s}^{-1} \text{ Mpc}^{-1}$, which are 14.1% and 14.8% better than those of CMB, respectively. Furthermore, the constraint precisions of Ω_m and H_0 using the CMB+Network data are 2.30% and 0.77%, respectively, which are worse

than the results by the 3G GW detector network given in ref. [67].

In figure 7, we show the constraint results in the Ω_m - w and w - H_0 planes for the w CDM model. We see that it is challenging to constrain the w CDM model by solely using the 2.5G GW bright sirens. Although the 3G GW detectors cannot precisely measure w as well, even the worst constraint from the Einstein Telescope (ET) is $\sigma(w) = 0.138$ [67], which is 76.4% better than that of Voyager-NEMO. In addition, the contours of CMB and Network show different parameter degeneracy orientations (almost orthogonal in the w - H_0 plane), and thus the combination of them could effectively break the cosmological parameter degeneracies. The combination of CMB and Network gives $\sigma(\Omega_m) = 0.011$, $\sigma(H_0) = 1.10 \text{ km s}^{-1} \text{ Mpc}^{-1}$, and $\sigma(w) = 0.045$, which are 84.3%, 85.8%, and 82.7% better than those of CMB, respectively. For the EoS parameter of dark energy, the precision can reach 4.50% using the combination of CMB and 2.5G GW bright sirens.

Since the constraint results by solely using the GW bright sirens are rather poor, we only show the combination results in the $w_0 w_a$ CDM model. In figure 8, we show the case in the w_0 - w_a plane for the $w_0 w_a$ CDM model using the CMB and CMB+Network data. Similarly, the constraints on w_0 and w_a by the 2.5G GW detectors are also much worse than those of the 3G GW detectors. The constraint on w_0 by ET is 74.8% better than that of the Voyager-NEMO network [67]. We see that the combination of CMB and 2.5G GW bright sirens can also break cosmological parameter degeneracies. The joint CMB+Network data give $\sigma(w_0) = 0.44$, which is 25.4% better than that of CMB. Furthermore, the single GW or CMB data cannot constrain w_a , the combination of CMB and Network gives $\sigma(w_a) = 1.6$, worse than the result by the Cosmic Explorer (CE) [67].

The above results show that the bright sirens from the 2.5G GW detectors can potentially help resolve the Hubble tension, but it is more helpful to consider the 2.5G GW detector network to perform the cosmological analysis. Nevertheless, it is challenging to precisely measure other cosmological parameters by solely using the 2.5G GW bright sirens. Fortunately, the parameter degeneracy orientations of CMB and bright sirens are different, and thus the combination of them could break the cosmological parameter degeneracies, especially in the dynamical dark energy models. In addition, the ability of the Voyager-NEMO network to constrain cosmological parameters is much worse than that of the 3G GW detectors. The constraint precisions on H_0 using the 3G GW detectors can improve by an order of magnitude compared to that obtained from the 2.5G GW detectors.

3.2 Dark sirens

In this subsection, we shall report the constraint results of the dark sirens. In figure 9, we show the constraint results of the scenarios of dark sirens, bright sirens, and bright and dark sirens from Voyager and the Voyager-NEMO network. We can see that Voyager could measure H_0 to a precision of 1.81%. The dark sirens from the Voyager-NEMO network can potentially constrain H_0 to a precision of 1.68%, which is comparable with the above bright siren result. Such precision is also one order of magnitude worse than those from the 3G GW detectors. Furthermore, we see that the best-fit results of dark sirens are offset from the preset value. The prime cause is that localization errors of dark sirens are large, and thus the wrong redshifts are obtained when statistically inferring the redshift information. As a result, this introduces the bias in the estimations of cosmological parameters. In addition, Ω_m cannot be well constrained due to the low-redshift dark sirens ($z < 0.15$).

In addition, LIGO-Virgo-KAGRA also gives the constraint on H_0 using the combination of bright and dark sirens with a precision of about 10% [74]. Therefore, we also forecast the

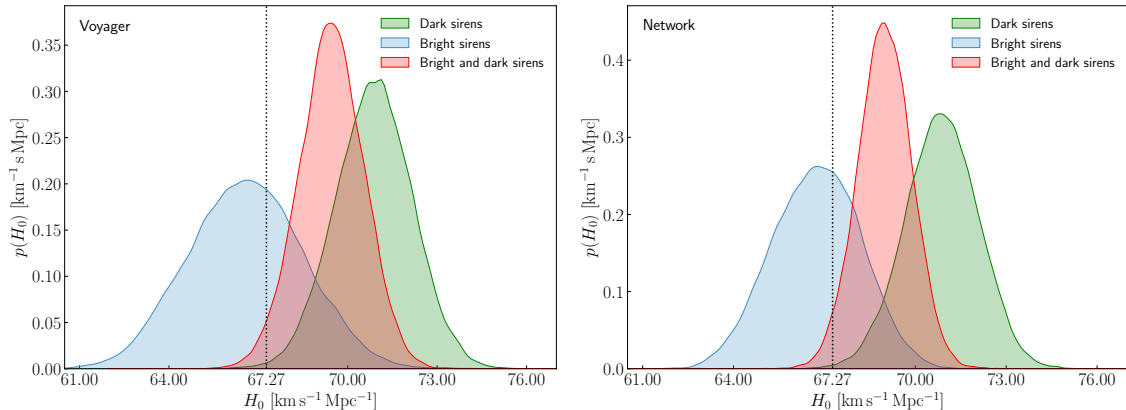


Figure 9. One-dimensional marginalized probability distributions for H_0 from dark sirens, bright sirens, and bright and dark sirens based on the 10-year observation of Voyager and the Voyager-NEMO network. Here the galaxy catalogs are uniformly simulated in a co-moving volume with a number density of 0.02 Mpc^{-3} , as described in section 2.5. The dotted line indicates the fiducial values of cosmological parameters preset in the simulation.

Table 3. Constraint results of the dark sirens and the combination of bright and dark sirens from Voyager and the Voyager-NEMO network based on the 10-year observation. The first column represents the detection strategy, the second column represents the number of the simulated dark siren data used in this work, the third to fifth columns represent the percentages of GW events with $N_{\text{in}} \leq 10$, $N_{\text{in}} \leq 100$, and $N_{\text{in}} \leq 1000$, the sixth and seventh column represents the relative errors of H_0 using dark sirens and the combination of bright and dark sirens. See section 3.1 for more details about bright sirens. Note that the relative errors of Ω_m are not shown due to the poor constraints.

Detection strategy	Number	$N_{\text{in}} \leq 10$	$N_{\text{in}} \leq 100$	$N_{\text{in}} \leq 1000$	$\varepsilon(H_0)$	
					Dark sirens	Bright and dark sirens
Voyager	83	1.20%	18.07%	96.39%	1.81%	1.55%
Network	93	1.08%	13.98%	96.77%	1.68%	1.27%

constraint on H_0 using the bright and dark sirens from the 2.5G GW detectors. The bright and dark sirens from the single Voyager observatory give a 1.55% measurement on H_0 . The constraint precision of H_0 is expected to reach 1.27% using the bright and dark sirens from the Voyager-NEMO network, better than the result of the distance ladder measurement [4]. We see that compared to the single Voyager, the constraint precision of H_0 using the Voyager-NEMO network can only have a slight improvement, because NEMO is mainly sensitive to the high-frequency BNS mergers. However, for the combination of bright and dark siren scenario, the improvement is significant, from 1.61% to 1.36%. In conclusion, it is worth expecting that the standard siren observations from the 2.5G GW detectors can play a crucial role in making an arbitration for the Hubble tension.

3.3 Impact of uncertainty in the BNS merger rate on estimating cosmological parameters

We investigate the impact of uncertainty in the BNS merger rate on the cosmological parameter estimations. Since the current inferred BBH merger rate has a small error range (no

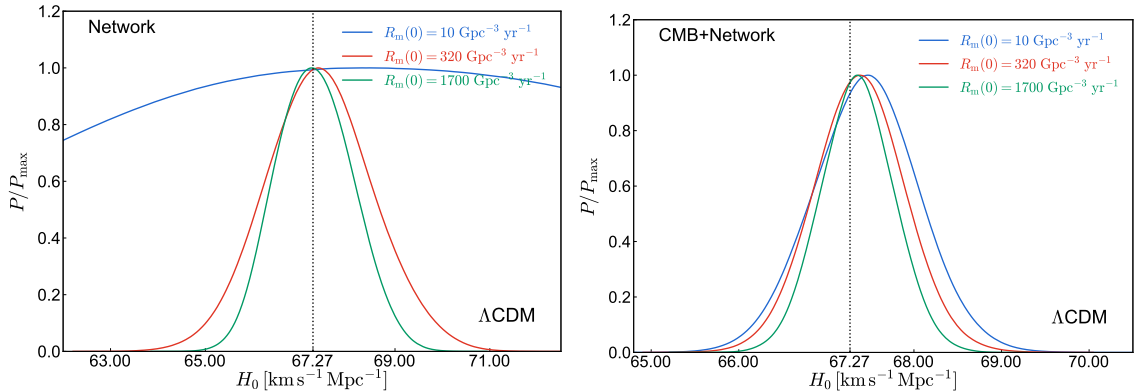


Figure 10. One-dimensional marginalized probability distributions for H_0 in the Λ CDM model based on the Voyager-NEMO network (10-year observation) and CMB+Network data in the scenarios of considering the BNS merger rates $R_m(0) = 10 \text{ Gpc}^{-3} \text{ yr}^{-1}$, $R_m(0) = 320 \text{ Gpc}^{-3} \text{ yr}^{-1}$, and $R_m(0) = 1700 \text{ Gpc}^{-3} \text{ yr}^{-1}$. Here, the dotted lines indicate the fiducial values of cosmological parameters preset in the simulation.

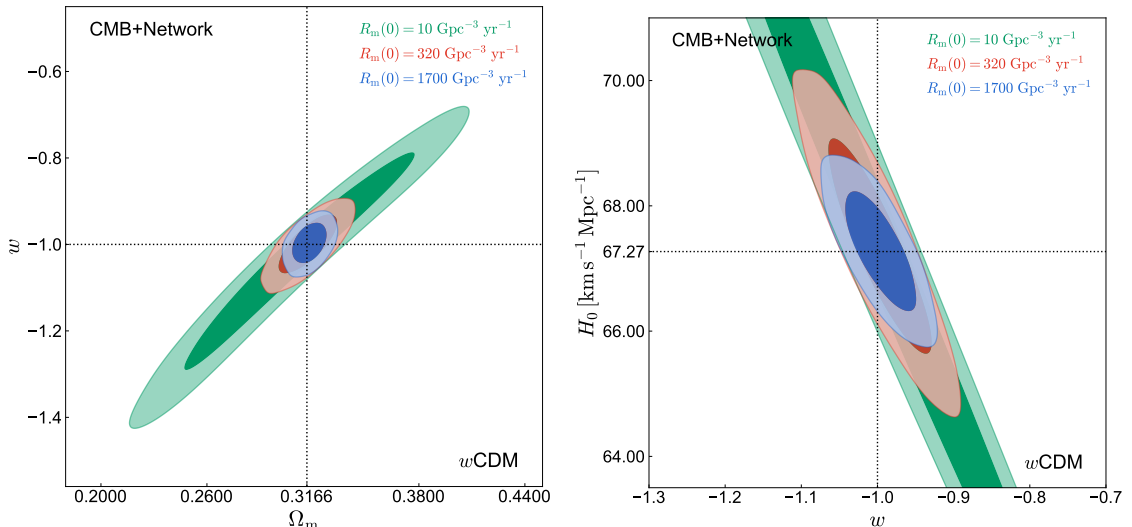


Figure 11. Two-dimensional marginalized contours (68.3% and 95.4% confidence level) in the Ω_m - w and w - H_0 planes in the w CDM model from the CMB+Network data in the scenarios of considering the BNS merger rates $R_m(0) = 10 \text{ Gpc}^{-3} \text{ yr}^{-1}$, $R_m(0) = 320 \text{ Gpc}^{-3} \text{ yr}^{-1}$, and $R_m(0) = 1700 \text{ Gpc}^{-3} \text{ yr}^{-1}$. Here, the dotted lines indicate the fiducial values of cosmological parameters preset in the simulation.

difference in magnitude), only BNS mergers are considered in this subsection. We consider the lower, medium, and upper limits of BNS merger rates given by the latest O3 observation from LIGO-Virgo-KAGRA [86], i.e., $R_m(0) = 10 \text{ Gpc}^{-3} \text{ yr}^{-1}$ (lower), $R_m(0) = 320 \text{ Gpc}^{-3} \text{ yr}^{-1}$ (medium, as discussed above), and $R_m(0) = 1700 \text{ Gpc}^{-3} \text{ yr}^{-1}$ (upper). A higher BNS merger rate leads to a higher detection rate of bright sirens and thus better constraints on the cosmological parameters.

In figure 10, we show the constraint results using the Network and CMB+Network data in the Λ CDM model. From the left panel, as clearly seen, bright sirens based on the

Table 4. Same as table 2, but using the Network and CMB+Network data based on the BNS merger rates $R_m(0) = 10 \text{ Gpc}^{-3} \text{ yr}^{-1}$ and $R_m(0) = 1700 \text{ Gpc}^{-3} \text{ yr}^{-1}$. Here H_0 is in units of $\text{km s}^{-1} \text{ Mpc}^{-1}$. Note that constraints on cosmological parameters based on $R_m(0) = 320 \text{ Gpc}^{-3} \text{ yr}^{-1}$ are shown in table 2.

Model	Error	Network		CMB+Network	
		$R_m(0) = 10$	$R_m(0) = 1700$	$R_m(0) = 10$	$R_m(0) = 1700$
Λ CDM	$\sigma(\Omega_m)$	–	0.0990	0.0085	0.0059
	$\sigma(H_0)$	5.30	0.82	0.61	0.42
	$\varepsilon(\Omega_m)$	–	31.94%	2.69%	1.86%
	$\varepsilon(H_0)$	7.59%	1.21%	0.90%	0.62%
w CDM	$\sigma(\Omega_m)$	–	0.1950	0.0410	0.0064
	$\sigma(H_0)$	–	1.10	4.85	0.64
	$\sigma(w)$	–	0.460	0.160	0.031
	$\varepsilon(\Omega_m)$	–	51.32%	13.18%	2.01%
	$\varepsilon(H_0)$	–	1.64%	7.09%	0.95%
	$\varepsilon(w)$	–	40.35%	15.53%	3.11%

lower merger rate cannot constrain H_0 . However, bright sirens based on the medium and upper merger rates can both give tight constraints on H_0 . With upper merger rate, bright sirens from Network are expected to constrain H_0 to a precision of 1.21%, better than the current distance ladder measurement [4]. When combining with CMB, tight constraint on H_0 could also be obtained, but the combined results based on the lower merger rate are mainly contributions from CMB. With the addition of the Network data with upper merger rate to CMB, the constraints on Ω_m and H_0 could be improved by 30.6% and 31.1%, respectively, because the parameter degeneracies generated by CMB are broken by GW.

Since the above results show that it is challenging to measure cosmological parameters in the dynamical dark energy models by solely using the bright sirens, we only show the case of the combination of GW and CMB, shown in figure 11. The detailed constraint results are shown in table 4. We can see that the ability of GW to break the cosmological parameter degeneracies is strong, even the bright sirens with lower merger rate can improve the cosmological parameter precisions to some extent. When combining the mock bright sirens from Network (lower merger rate) with CMB, the constraints on Ω_m , H_0 , and w can be improved by 41.4%, 37.4%, and 38.5%, respectively. While for the upper merger rate case, the improvements on Ω_m , H_0 , and w are 90.9%, 91.7%, and 88.1%, respectively. Moreover, the constraint precision of w using the CMB+Network data with upper merger rate is 3.11%, close to the latest CMB+SN result [109]. We can conclude that the BNS merger rates can seriously affect the cosmological parameter estimations, but the 2.5G GW standard sirens hold promise in helping address the Hubble tension.

3.4 Impact of the detector coordinates in the antenna response functions on estimating the Hubble constant in the dark siren scenario

In this work, we do not consider the detector coordinates in the antenna response functions, which can impact the GW localization and the dark siren analysis. Hence, we wish to

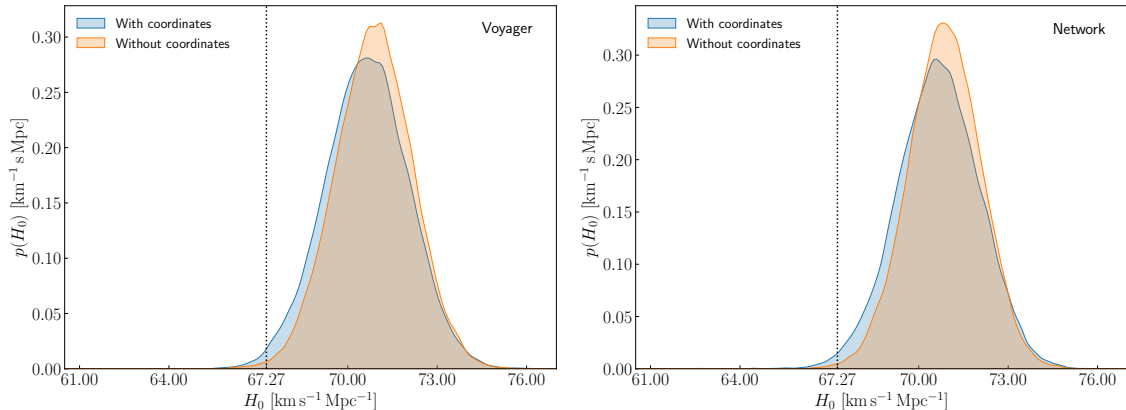


Figure 12. Same as figure 9, but for the scenario with and without considering the detector coordinates in the antenna response functions.

Table 5. Same as table 3, but considers the detector coordinates in the antenna response functions for the dark siren results.

Detection strategy	Number	$N_{\text{in}} \leq 10$	$N_{\text{in}} \leq 100$	$N_{\text{in}} \leq 1000$	$\varepsilon(H_0)$
Voyager	73	1.37%	20.55%	98.63%	1.97%
Network	76	1.32%	19.74%	98.68%	1.93%

show the impact of the detector coordinates in the antenna response functions on estimating H_0 in the dark siren analysis. Since the detailed coordinates of Voyager and NEMO are currently uncertain, we make an assumption that the coordinates of Voyager and NEMO are the same as those of CE in the US and CE in Australia (detailed coordinates can be found in e.g., ref. [65]), respectively. In figure 12, we show the one-dimensional marginalized probability distributions for H_0 with and without considering the detector coordinates in the antenna response functions. As clearly seen, the scenario without detector coordinates gives tighter constraints than those with detector coordinates. Concretely, when considering the detector coordinates in the antenna response functions, H_0 can be constrained to precisions of 1.97% and 1.93% using Voyager and the Voyager-NEMO network, respectively. The prime cause is that the numbers of dark sirens obtained by considering the detector coordinates are less than those without considering. After considering the detector coordinates, the constraints on H_0 are 8.1% and 12.4% worse than those without considering for Voyager and the Voyager-NEMO network, respectively. In conclusion, worse constraints can be obtained if the detector coordinates are considered in the antenna response functions. This work shows the optimistic scenario of the 2.5G GW detectors in the cosmological parameter estimations.

4 Conclusion

In this work, we explore the potential of the 2.5G ground-based GW detectors by considering three detection strategies: Voyager, NEMO, and the Voyager-NEMO network, in constraining cosmological parameters, based on the 10-year observation. Our main analysis

is based on the BNS merger rate $R_m(0) = 320 \text{ Gpc}^{-3} \text{ yr}^{-1}$. Furthermore, the impact of uncertainty in the BNS merger rate on estimating cosmological parameters is also discussed. We consider the optimistic scenario in which EM counterparts (SGRBs) can be detected and the conservative scenario in which EM counterparts are not available to perform cosmological analysis. For the simulation of the bright siren data, we calculate the expected detection distributions of GW-SGRB events. We consider the THESEUS-like mission as the representative of the SGRB detector. We consider three typical dark energy models, i.e., the Λ CDM, w CDM, and w_0w_a CDM models, to make the cosmological analysis. In the conservative scenario, we choose the dark siren events with $\text{SNR} \geq 100$ combined with the simulated galaxy catalogs to estimate cosmological parameters in the Λ CDM model.

The mock bright siren data from Voyager, NEMO, and the Voyager-NEMO network can potentially measure H_0 to precisions of 2.08%, 6.44%, and 1.63%, respectively, but it is rather challenging to measure other cosmological parameters by solely using the mock 2.5G bright siren data. Fortunately, the cosmological parameter degeneracy orientations of bright sirens and CMB are different, and thus the combination of them could break the cosmological parameter degeneracies, especially in the dynamical dark energy models. Moreover, compared to the CMB data, the improvements on Ω_m , H_0 , and w constraints using CMB+Network are 84.3%, 85.8%, and 82.7%, respectively. For the w_0w_a CDM model, the joint CMB+Network data give $\sigma(w_0) = 0.44$ and $\sigma(w_a) = 1.6$.

For the mock 2.5G dark siren scenario, H_0 is potentially measured to precisions of 1.81% and 1.68% using Voyager and the Voyager-NEMO network, respectively, which is comparable with the results by the mock 2.5G bright sirens. When combining dark sirens with bright sirens, H_0 is expected to reach precisions of 1.55% and 1.27% for Voyager and the Voyager-NEMO network, respectively, which are close to or better than the distance ladder measurement. In addition, the ability of the standard sirens from the Voyager-NEMO network to constrain cosmological parameters is much worse than those of the 3G GW detectors.

We discuss the impact of uncertainty in the BNS merger rate on estimating cosmological parameters. We find that the BNS merger rates can severely affect the cosmological parameter estimations (measurement precisions of H_0 from 7.59% to 1.21%). Even in the scenario of the lower BNS merger rate, the ability of 2.5G bright sirens to break the cosmological parameter degeneracies is strong in the w CDM model, but main contributions of CMB+Network in the Λ CDM model come from CMB. In addition, we also discuss the impact of the detector coordinates in the antenna response functions on estimating H_0 in the dark siren scenario. We find that worse constraints can be obtained if the detector coordinates are considered in the antenna response functions. Our constraint results are optimistic estimations.

We can conclude that (i) it is more helpful to consider the 2.5G detector network than the single 2.5G GW observatory for the cosmological research, (ii) the bright sirens from the 2.5G GW detectors could provide precise measurements on the Hubble constant (a potential 1.63% measurement), but are poor at measuring other cosmological parameters, (iii) the bright sirens from the 2.5G GW detectors could effectively break the cosmological parameter degeneracies generated by the CMB data and thus the combination of them could improve the measurement precisions of cosmological parameters, especially in the dynamical dark energy models, and (iiii) the mock dark sirens from the 2.5G GW detectors give comparable constraint on the Hubble constant (a potential 1.68% measurement) with the mock 2.5G bright sirens, while the combination of the bright and dark sirens can measure the Hubble constant to a precision of 1.27%. It is worth expecting that the Hubble tension could be resolved in the era of the 2.5G ground-based GW detectors.

Acknowledgments

We thank the anonymous referee for the useful comments and Yue-Yan Dong for the fruitful discussions. In addition, we thank Paul D. Lasky for providing the sensitivity curve of NEMO. This work was supported by the National SKA Program of China (Grants Nos. 2022SKA0110200 and 2022SKA0110203) and the National Natural Science Foundation of China (Grants Nos. 11975072, 11875102, and 11835009).

References

- [1] WMAP collaboration, *First year Wilkinson Microwave Anisotropy Probe (WMAP) observations: Determination of cosmological parameters*, *Astrophys. J. Suppl.* **148** (2003) 175 [[astro-ph/0302209](#)].
- [2] WMAP collaboration, *First year Wilkinson Microwave Anisotropy Probe (WMAP) observations: Preliminary maps and basic results*, *Astrophys. J. Suppl.* **148** (2003) 1 [[astro-ph/0302207](#)].
- [3] PLANCK collaboration, *Planck 2018 results. VI. Cosmological parameters*, *Astron. Astrophys.* **641** (2020) A6 [[1807.06209](#)].
- [4] A.G. Riess et al., *A Comprehensive Measurement of the Local Value of the Hubble Constant with $1 \text{ km s}^{-1} \text{ Mpc}^{-1}$ Uncertainty from the Hubble Space Telescope and the SH0ES Team*, *Astrophys. J. Lett.* **934** (2022) L7 [[2112.04510](#)].
- [5] L. Verde, T. Treu and A.G. Riess, *Tensions between the Early and the Late Universe*, *Nature Astron.* **3** (2019) 891 [[1907.10625](#)].
- [6] A.G. Riess, *The Expansion of the Universe is Faster than Expected*, *Nature Rev. Phys.* **2** (2019) 10 [[2001.03624](#)].
- [7] E. Di Valentino, O. Mena, S. Pan, L. Visinelli, W. Yang, A. Melchiorri et al., *In the realm of the Hubble tension—a review of solutions*, *Class. Quant. Grav.* **38** (2021) 153001 [[2103.01183](#)].
- [8] M. Kamionkowski and A.G. Riess, *The Hubble Tension and Early Dark Energy*, *Ann. Rev. Nucl. Part. Sci.* **73** (2023) 153 [[2211.04492](#)].
- [9] L. Perivolaropoulos and F. Skara, *Challenges for Λ CDM: An update*, *New Astron. Rev.* **95** (2022) 101659 [[2105.05208](#)].
- [10] E. Abdalla et al., *Cosmology intertwined: A review of the particle physics, astrophysics, and cosmology associated with the cosmological tensions and anomalies*, *JHEAp* **34** (2022) 49 [[2203.06142](#)].
- [11] R.-Y. Guo, J.-F. Zhang and X. Zhang, *Can the H_0 tension be resolved in extensions to Λ CDM cosmology?*, *JCAP* **02** (2019) 054 [[1809.02340](#)].
- [12] V. Poulin, T.L. Smith, T. Karwal and M. Kamionkowski, *Early Dark Energy Can Resolve The Hubble Tension*, *Phys. Rev. Lett.* **122** (2019) 221301 [[1811.04083](#)].
- [13] R.-G. Cai, Z.-K. Guo, L. Li, S.-J. Wang and W.-W. Yu, *Chameleon dark energy can resolve the Hubble tension*, *Phys. Rev. D* **103** (2021) 121302 [[2102.02020](#)].
- [14] L.-Y. Gao, Z.-W. Zhao, S.-S. Xue and X. Zhang, *Relieving the H_0 tension with a new interacting dark energy model*, *JCAP* **07** (2021) 005 [[2101.10714](#)].
- [15] W. Yang, S. Pan, E. Di Valentino, R.C. Nunes, S. Vagnozzi and D.F. Mota, *Tale of stable interacting dark energy, observational signatures, and the H_0 tension*, *JCAP* **09** (2018) 019 [[1805.08252](#)].

- [16] E. Di Valentino, A. Melchiorri, O. Mena and S. Vagnozzi, *Nonminimal dark sector physics and cosmological tensions*, *Phys. Rev. D* **101** (2020) 063502 [[1910.09853](#)].
- [17] E. Di Valentino et al., *Snowmass2021 - Letter of interest cosmology intertwined II: The hubble constant tension*, *Astropart. Phys.* **131** (2021) 102605 [[2008.11284](#)].
- [18] M. Liu, Z. Huang, X. Luo, H. Miao, N.K. Singh and L. Huang, *Can Non-standard Recombination Resolve the Hubble Tension?*, *Sci. China Phys. Mech. Astron.* **63** (2020) 290405 [[1912.00190](#)].
- [19] X. Zhang and Q.-G. Huang, *Measuring H_0 from low- z datasets*, *Sci. China Phys. Mech. Astron.* **63** (2020) 290402 [[1911.09439](#)].
- [20] Q. Ding, T. Nakama and Y. Wang, *A gigaparsec-scale local void and the Hubble tension*, *Sci. China Phys. Mech. Astron.* **63** (2020) 290403 [[1912.12600](#)].
- [21] H. Li and X. Zhang, *A novel method of measuring cosmological distances using broad-line regions of quasars*, *Sci. Bull.* **65** (2020) 1419 [[2005.10458](#)].
- [22] S. Vagnozzi, F. Pacucci and A. Loeb, *Implications for the Hubble tension from the ages of the oldest astrophysical objects*, *JHEAp* **36** (2022) 27 [[2105.10421](#)].
- [23] R.-Y. Guo, J.-F. Zhang and X. Zhang, *Inflation model selection revisited after a 1.91% measurement of the Hubble constant*, *Sci. China Phys. Mech. Astron.* **63** (2020) 290406 [[1910.13944](#)].
- [24] L. Feng, D.-Z. He, H.-L. Li, J.-F. Zhang and X. Zhang, *Constraints on active and sterile neutrinos in an interacting dark energy cosmology*, *Sci. China Phys. Mech. Astron.* **63** (2020) 290404 [[1910.03872](#)].
- [25] L.-Y. Gao, S.-S. Xue and X. Zhang, *Dark energy and matter interacting scenario can relieve H_0 and S_8 tensions*, **2212.13146**.
- [26] B.F. Schutz, *Determining the Hubble Constant from Gravitational Wave Observations*, *Nature* **323** (1986) 310.
- [27] D.E. Holz and S.A. Hughes, *Using gravitational-wave standard sirens*, *Astrophys. J.* **629** (2005) 15 [[astro-ph/0504616](#)].
- [28] S. Nissanke, D.E. Holz, S.A. Hughes, N. Dalal and J.L. Sievers, *Exploring short gamma-ray bursts as gravitational-wave standard sirens*, *Astrophys. J.* **725** (2010) 496 [[0904.1017](#)].
- [29] N. Dalal, D.E. Holz, S.A. Hughes and B. Jain, *Short grb and binary black hole standard sirens as a probe of dark energy*, *Phys. Rev. D* **74** (2006) 063006 [[astro-ph/0601275](#)].
- [30] H.-Y. Chen, M. Fishbach and D.E. Holz, *A two per cent Hubble constant measurement from standard sirens within five years*, *Nature* **562** (2018) 545 [[1712.06531](#)].
- [31] C. Cutler and D.E. Holz, *Ultra-high precision cosmology from gravitational waves*, *Phys. Rev. D* **80** (2009) 104009 [[0906.3752](#)].
- [32] R.-G. Cai and T. Yang, *Estimating cosmological parameters by the simulated data of gravitational waves from the Einstein Telescope*, *Phys. Rev. D* **95** (2017) 044024 [[1608.08008](#)].
- [33] R.-G. Cai, Z. Cao, Z.-K. Guo, S.-J. Wang and T. Yang, *The Gravitational-Wave Physics*, *Natl. Sci. Rev.* **4** (2017) 687 [[1703.00187](#)].
- [34] R. Gray et al., *Cosmological inference using gravitational wave standard sirens: A mock data analysis*, *Phys. Rev. D* **101** (2020) 122001 [[1908.06050](#)].
- [35] S. Vitale and H.-Y. Chen, *Measuring the Hubble constant with neutron star black hole mergers*, *Phys. Rev. Lett.* **121** (2018) 021303 [[1804.07337](#)].
- [36] M. Lagos, M. Fishbach, P. Landry and D.E. Holz, *Standard sirens with a running Planck mass*, *Phys. Rev. D* **99** (2019) 083504 [[1901.03321](#)].

- [37] S. Camera and A. Nishizawa, *Beyond Concordance Cosmology with Magnification of Gravitational-Wave Standard Sirens*, *Phys. Rev. Lett.* **110** (2013) 151103 [[1303.5446](#)].
- [38] S. Mukherjee, G. Lavaux, F.R. Bouchet, J. Jasche, B.D. Wandelt, S.M. Nissanke et al., *Velocity correction for Hubble constant measurements from standard sirens*, *Astron. Astrophys.* **646** (2021) A65 [[1909.08627](#)].
- [39] R. D’Agostino and R.C. Nunes, *Probing observational bounds on scalar-tensor theories from standard sirens*, *Phys. Rev. D* **100** (2019) 044041 [[1907.05516](#)].
- [40] L.-F. Wang, X.-N. Zhang, J.-F. Zhang and X. Zhang, *Impacts of gravitational-wave standard siren observation of the Einstein Telescope on weighing neutrinos in cosmology*, *Phys. Lett. B* **782** (2018) 87 [[1802.04720](#)].
- [41] R.-G. Cai, T.-B. Liu, X.-W. Liu, S.-J. Wang and T. Yang, *Probing cosmic anisotropy with gravitational waves as standard sirens*, *Phys. Rev. D* **97** (2018) 103005 [[1712.00952](#)].
- [42] S.-J. Jin, D.-Z. He, Y. Xu, J.-F. Zhang and X. Zhang, *Forecast for cosmological parameter estimation with gravitational-wave standard siren observation from the Cosmic Explorer*, *JCAP* **03** (2020) 051 [[2001.05393](#)].
- [43] E. Belgacem, Y. Dirian, S. Foffa, E.J. Howell, M. Maggiore and T. Regimbau, *Cosmology and dark energy from joint gravitational wave-GRB observations*, *JCAP* **08** (2019) 015 [[1907.01487](#)].
- [44] C. Howlett and T.M. Davis, *Standard siren speeds: improving velocities in gravitational-wave measurements of H_0* , *Mon. Not. Roy. Astron. Soc.* **492** (2020) 3803 [[1909.00587](#)].
- [45] J.-F. Zhang, M. Zhang, S.-J. Jin, J.-Z. Qi and X. Zhang, *Cosmological parameter estimation with future gravitational wave standard siren observation from the Einstein Telescope*, *JCAP* **09** (2019) 068 [[1907.03238](#)].
- [46] P.-J. Wu, Y. Shao, S.-J. Jin and X. Zhang, *A path to precision cosmology: synergy between four promising late-universe cosmological probes*, *JCAP* **06** (2023) 052 [[2202.09726](#)].
- [47] J.M. Ezquiaga and D.E. Holz, *Spectral Sirens: Cosmology from the Full Mass Distribution of Compact Binaries*, *Phys. Rev. Lett.* **129** (2022) 061102 [[2202.08240](#)].
- [48] L.-F. Wang, Z.-W. Zhao, J.-F. Zhang and X. Zhang, *A preliminary forecast for cosmological parameter estimation with gravitational-wave standard sirens from TianQin*, *JCAP* **11** (2020) 012 [[1907.01838](#)].
- [49] Z.-W. Zhao, L.-F. Wang, J.-F. Zhang and X. Zhang, *Prospects for improving cosmological parameter estimation with gravitational-wave standard sirens from Taiji*, *Sci. Bull.* **65** (2020) 1340 [[1912.11629](#)].
- [50] L.-F. Wang, S.-J. Jin, J.-F. Zhang and X. Zhang, *Forecast for cosmological parameter estimation with gravitational-wave standard sirens from the LISA-Taiji network*, *Sci. China Phys. Mech. Astron.* **65** (2022) 210411 [[2101.11882](#)].
- [51] S.-J. Jin, L.-F. Wang, P.-J. Wu, J.-F. Zhang and X. Zhang, *How can gravitational-wave standard sirens and 21-cm intensity mapping jointly provide a precise late-universe cosmological probe?*, *Phys. Rev. D* **104** (2021) 103507 [[2106.01859](#)].
- [52] J. Yu, H. Song, S. Ai, H. Gao, F. Wang, Y. Wang et al., *Multimessenger Detection Rates and Distributions of Binary Neutron Star Mergers and Their Cosmological Implications*, *Astrophys. J.* **916** (2021) 54 [[2104.12374](#)].
- [53] H.-Y. Chen, C. Talbot and E.A. Chase, *Mitigating the counterpart selection effect for standard sirens*, [2307.10402](#).
- [54] LISA COSMOLOGY WORKING GROUP collaboration, *Cosmology with the Laser Interferometer Space Antenna*, *Living Rev. Rel.* **26** (2023) 5 [[2204.05434](#)].

- [55] A. Dhani, S. Borhanian, A. Gupta and B. Sathyaprakash, *Cosmography with bright and Love sirens*, [2212.13183](#).
- [56] L.-G. Zhu, L.-H. Xie, Y.-M. Hu, S. Liu, E.-K. Li, N.R. Napolitano et al., *Constraining the Hubble constant to a precision of about 1% using multi-band dark standard siren detections*, *Sci. China Phys. Mech. Astron.* **65** (2022) 259811 [[2110.05224](#)].
- [57] J.-Z. Qi, S.-J. Jin, X.-L. Fan, J.-F. Zhang and X. Zhang, *Using a multi-messenger and multi-wavelength observational strategy to probe the nature of dark energy through direct measurements of cosmic expansion history*, *JCAP* **12** (2021) 042 [[2102.01292](#)].
- [58] S.-J. Jin, R.-Q. Zhu, L.-F. Wang, H.-L. Li, J.-F. Zhang and X. Zhang, *Impacts of gravitational-wave standard siren observations from Einstein Telescope and Cosmic Explorer on weighing neutrinos in interacting dark energy models*, *Commun. Theor. Phys.* **74** (2022) 105404 [[2204.04689](#)].
- [59] L.-F. Wang, Y. Shao, J.-F. Zhang and X. Zhang, *Ultra-low-frequency gravitational waves from individual supermassive black hole binaries as standard sirens*, [2201.00607](#).
- [60] J.-Y. Song, L.-F. Wang, Y. Li, Z.-W. Zhao, J.-F. Zhang, W. Zhao et al., *Synergy between CSST galaxy survey and gravitational-wave observation: Inferring the Hubble constant from dark standard sirens*, *Sci. China Phys. Mech. Astron.* **67** (2024) 230411 [[2212.00531](#)].
- [61] S.-J. Jin, S.-S. Xing, Y. Shao, J.-F. Zhang and X. Zhang, *Joint constraints on cosmological parameters using future multi-band gravitational wave standard siren observations**, *Chin. Phys. C* **47** (2023) 065104 [[2301.06722](#)].
- [62] W.-T. Hou, J.-Z. Qi, T. Han, J.-F. Zhang, S. Cao and X. Zhang, *Prospects for constraining interacting dark energy models from gravitational wave and gamma ray burst joint observation*, *JCAP* **05** (2023) 017 [[2211.10087](#)].
- [63] S. Borhanian, A. Dhani, A. Gupta, K.G. Arun and B.S. Sathyaprakash, *Dark Sirens to Resolve the Hubble–Lemaître Tension*, *Astrophys. J. Lett.* **905** (2020) L28 [[2007.02883](#)].
- [64] S.-J. Jin, Y.-Z. Zhang, J.-Y. Song, J.-F. Zhang and X. Zhang, *Taiji-TianQin-LISA network: Precisely measuring the Hubble constant using both bright and dark sirens*, *Sci. China Phys. Mech. Astron.* **67** (2024) 220412 [[2305.19714](#)].
- [65] S.-J. Jin, T.-N. Li, J.-F. Zhang and X. Zhang, *Prospects for measuring the Hubble constant and dark energy using gravitational-wave dark sirens with neutron star tidal deformation*, *JCAP* **08** (2023) 070 [[2202.11882](#)].
- [66] L.-G. Zhu and X. Chen, *The Dark Side of Using Dark Sirens to Constrain the Hubble–Lemaître Constant*, *Astrophys. J.* **948** (2023) 26 [[2302.10621](#)].
- [67] T. Han, S.-J. Jin, J.-F. Zhang and X. Zhang, *A comprehensive forecast for cosmological parameter estimation using joint observations of gravitational-wave standard sirens and short γ -ray bursts*, [2309.14965](#).
- [68] T.-N. Li, S.-J. Jin, H.-L. Li, J.-F. Zhang and X. Zhang, *Prospects for Probing the Interaction between Dark Energy and Dark Matter Using Gravitational-wave Dark Sirens with Neutron Star Tidal Deformation*, *Astrophys. J.* **963** (2024) 52 [[2310.15879](#)].
- [69] N. Muttoni, D. Laghi, N. Tamanini, S. Marsat and D. Izquierdo-Villalba, *Dark siren cosmology with binary black holes in the era of third-generation gravitational wave detectors*, *Phys. Rev. D* **108** (2023) 043543 [[2303.10693](#)].
- [70] M. Branchesi et al., *Science with the Einstein Telescope: a comparison of different designs*, *JCAP* **07** (2023) 068 [[2303.15923](#)].
- [71] LIGO SCIENTIFIC, VIRGO collaboration, *GW170817: Observation of Gravitational Waves from a Binary Neutron Star Inspiral*, *Phys. Rev. Lett.* **119** (2017) 161101 [[1710.05832](#)].

- [72] LIGO SCIENTIFIC, VIRGO, FERMI GBM, INTEGRAL, ICECUBE, ASTRO SAT CADMIUM ZINC TELLURIDE IMAGER TEAM, IPN, INSIGHT-HXMT, ANTARES, SWIFT, AGILE TEAM, 1M2H TEAM, DARK ENERGY CAMERA GW-EM, DES, DLT40, GRAWITA, FERMI-LAT, ATCA, ASKAP, LAS CUMBRES OBSERVATORY GROUP, OzGRAV, DWF (DEEPER WIDER FASTER PROGRAM), AST3, CAASTRO, VINROUGE, MASTER, J-GEM, GROWTH, JAGWAR, CALTECHNRAO, TTU-NRAO, NUSTAR, PAN-STARRS, MAXI TEAM, TZAC CONSORTIUM, KU, NORDIC OPTICAL TELESCOPE, EPESSTO, GROND, TEXAS TECH UNIVERSITY, SALT GROUP, TOROS, BOOTES, MWA, CALET, IKI-GW FOLLOW-UP, H.E.S.S., LOFAR, LWA, HAWC, PIERRE AUGER, ALMA, EURO VLBI TEAM, PI OF SKY, CHANDRA TEAM AT MCGILL UNIVERSITY, DFN, ATLAS TELESCOPES, HIGH TIME RESOLUTION UNIVERSE SURVEY, RIMAS, RATIR, SKA SOUTH AFRICA/MEERKAT collaboration, *Multi-messenger Observations of a Binary Neutron Star Merger*, *Astrophys. J. Lett.* **848** (2017) L12 [[1710.05833](#)].
- [73] LIGO SCIENTIFIC, VIRGO, 1M2H, DARK ENERGY CAMERA GW-E, DES, DLT40, LAS CUMBRES OBSERVATORY, VINROUGE, MASTER collaboration, *A gravitational-wave standard siren measurement of the Hubble constant*, *Nature* **551** (2017) 85 [[1710.05835](#)].
- [74] LIGO SCIENTIFIC, VIRGO,, KAGRA, VIRGO collaboration, *Constraints on the Cosmic Expansion History from GWTC-3*, *Astrophys. J.* **949** (2023) 76 [[2111.03604](#)].
- [75] LIGO collaboration, *A cryogenic silicon interferometer for gravitational-wave detection*, *Class. Quant. Grav.* **37** (2020) 165003 [[2001.11173](#)].
- [76] K. Ackley et al., *Neutron Star Extreme Matter Observatory: A kilohertz-band gravitational-wave detector in the global network*, *Publ. Astron. Soc. Austral.* **37** (2020) e047 [[2007.03128](#)].
- [77] M. Evans et al., *A Horizon Study for Cosmic Explorer: Science, Observatories, and Community*, [2109.09882](#).
- [78] N. Sarin and P.D. Lasky, *Multimessenger astronomy with a kHz-band gravitational-wave observatory*, *Publ. Astron. Soc. Austral.* **39** (2022) e007 [[2110.10892](#)].
- [79] S.W. Ballmer et al., *Snowmass2021 Cosmic Frontier White Paper: Future Gravitational-Wave Detector Facilities*, in *Snowmass 2021*, 3, 2022 [[2203.08228](#)].
- [80] P. Relton and V. Raymond, *Parameter estimation bias from overlapping binary black hole events in second generation interferometers*, *Phys. Rev. D* **104** (2021) 084039 [[2103.16225](#)].
- [81] S. Borhanian and B.S. Sathyaprakash, *Listening to the Universe with Next Generation Ground-Based Gravitational-Wave Detectors*, [2202.11048](#).
- [82] P. Madau and M. Dickinson, *Cosmic Star Formation History*, *Ann. Rev. Astron. Astrophys.* **52** (2014) 415 [[1403.0007](#)].
- [83] S. Vitale, W.M. Farr, K. Ng and C.L. Rodriguez, *Measuring the star formation rate with gravitational waves from binary black holes*, *Astrophys. J. Lett.* **886** (2019) L1 [[1808.00901](#)].
- [84] LIGO SCIENTIFIC, VIRGO collaboration, *GWTC-2: Compact Binary Coalescences Observed by LIGO and Virgo During the First Half of the Third Observing Run*, *Phys. Rev. X* **11** (2021) 021053 [[2010.14527](#)].
- [85] LIGO SCIENTIFIC, VIRGO collaboration, *Population Properties of Compact Objects from the Second LIGO-Virgo Gravitational-Wave Transient Catalog*, *Astrophys. J. Lett.* **913** (2021) L7 [[2010.14533](#)].
- [86] KAGRA, VIRGO, LIGO SCIENTIFIC collaboration, *Population of Merging Compact Binaries Inferred Using Gravitational Waves through GWTC-3*, *Phys. Rev. X* **13** (2023) 011048 [[2111.03634](#)].

- [87] H.-S. Cho, *Parameter estimation using a complete signal and inspiral templates for low mass binary black holes with Advanced LIGO sensitivity*, *Class. Quant. Grav.* **32** (2015) 235007 [[1502.04399](#)].
- [88] P. Kumar, T. Chu, H. Fong, H.P. Pfeiffer, M. Boyle, D.A. Hemberger et al., *Accuracy of binary black hole waveform models for aligned-spin binaries*, *Phys. Rev. D* **93** (2016) 104050 [[1601.05396](#)].
- [89] B.S. Sathyaprakash and B.F. Schutz, *Physics, Astrophysics and Cosmology with Gravitational Waves*, *Living Rev. Rel.* **12** (2009) 2 [[0903.0338](#)].
- [90] L. Blanchet and B.R. Iyer, *Hadamard regularization of the third post-Newtonian gravitational wave generation of two point masses*, *Phys. Rev. D* **71** (2005) 024004 [[gr-qc/0409094](#)].
- [91] K.G. Arun, B.R. Iyer, B.S. Sathyaprakash and P.A. Sundararajan, *Parameter estimation of inspiralling compact binaries using 3.5 post-Newtonian gravitational wave phasing: The Non-spinning case*, *Phys. Rev. D* **71** (2005) 084008 [[gr-qc/0411146](#)].
- [92] T. Robson, N.J. Cornish and C. Liu, *The construction and use of LISA sensitivity curves*, *Class. Quant. Grav.* **36** (2019) 105011 [[1803.01944](#)].
- [93] “LIGO Document T1500293-v13.” <https://dcc.ligo.org/LIGO-T1500293/public>.
- [94] N. Tamanini, C. Caprini, E. Barausse, A. Sesana, A. Klein and A. Petiteau, *Science with the space-based interferometer eLISA. III: Probing the expansion of the Universe using gravitational wave standard sirens*, *JCAP* **04** (2016) 002 [[1601.07112](#)].
- [95] L. Speri, N. Tamanini, R.R. Caldwell, J.R. Gair and B. Wang, *Testing the Quasar Hubble Diagram with LISA Standard Sirens*, *Phys. Rev. D* **103** (2021) 083526 [[2010.09049](#)].
- [96] C.M. Hirata, D.E. Holz and C. Cutler, *Reducing the weak lensing noise for the gravitational wave Hubble diagram using the non-Gaussianity of the magnification distribution*, *Phys. Rev. D* **81** (2010) 124046 [[1004.3988](#)].
- [97] B. Kocsis, Z. Frei, Z. Haiman and K. Menou, *Finding the electromagnetic counterparts of cosmological standard sirens*, *Astrophys. J.* **637** (2006) 27 [[astro-ph/0505394](#)].
- [98] J.-h. He, *Accurate method to determine the systematics due to the peculiar velocities of galaxies in measuring the Hubble constant from gravitational-wave standard sirens*, *Phys. Rev. D* **100** (2019) 023527 [[1903.11254](#)].
- [99] P. Meszaros and A. Meszaros, *The Brightness distribution of bursting sources in relativistic cosmologies*, *Astrophys. J.* **449** (1995) 9 [[astro-ph/9503087](#)].
- [100] A. Meszaros, J. Ripa and F. Ryde, *Cosmological effects on the observed flux and fluence distributions of gamma-ray bursts: Are the most distant bursts in general the faintest ones?*, *Astron. Astrophys.* **529** (2011) A55 [[1101.5040](#)].
- [101] D.L. Band, *Comparison of the gamma-ray burst sensitivity of different detectors*, *Astrophys. J.* **588** (2003) 945 [[astro-ph/0212452](#)].
- [102] D. Wanderman and T. Piran, *The rate, luminosity function and time delay of non-Collapsar short GRBs*, *Mon. Not. Roy. Astron. Soc.* **448** (2015) 3026 [[1405.5878](#)].
- [103] H.-Y. Chen, P.S. Cowperthwaite, B.D. Metzger and E. Berger, *A Program for Multimessenger Standard Siren Cosmology in the Era of LIGO A+, Rubin Observatory, and Beyond*, *Astrophys. J. Lett.* **908** (2021) L4 [[2011.01211](#)].
- [104] S. Ronchini, M. Branchesi, G. Oganesyan, B. Banerjee, U. Dupletsa, G. Ghirlanda et al., *Perspectives for multimessenger astronomy with the next generation of gravitational-wave detectors and high-energy satellites*, *Astron. Astrophys.* **665** (2022) A97 [[2204.01746](#)].
- [105] D. Foreman-Mackey, D.W. Hogg, D. Lang and J. Goodman, *emcee: The MCMC Hammer*, *Publ. Astron. Soc. Pac.* **125** (2013) 306 [[1202.3665](#)].

- [106] E. Barausse, *The evolution of massive black holes and their spins in their galactic hosts*, *Mon. Not. Roy. Astron. Soc.* **423** (2012) 2533 [[1201.5888](#)].
- [107] I. Mandel, W.M. Farr and J.R. Gair, *Extracting distribution parameters from multiple uncertain observations with selection biases*, *Mon. Not. Roy. Astron. Soc.* **486** (2019) 1086 [[1809.02063](#)].
- [108] L. Chen, Q.-G. Huang and K. Wang, *Distance Priors from Planck Final Release*, *JCAP* **02** (2019) 028 [[1808.05724](#)].
- [109] D. Brout et al., *The Pantheon+ Analysis: Cosmological Constraints*, *Astrophys. J.* **938** (2022) 110 [[2202.04077](#)].